Plane-Based Calibration of Central Catadioptric Cameras

Simone Gasparini, Peter Sturm, Joao Barreto

HAL Id: inria-00586972
https://hal.inria.fr/inria-00586972

Submitted on 19 Apr 2011

Plane-Based Calibration of Central Catadioptric Cameras

Simone Gasparini, Peter Sturm
INRIA Grenoble–Rhône-Alpes
655 Avenue de l'Europe
38334 Montbonnot St. Martin, France
{name.surname}@inrialpes.fr

João P. Barreto
Institute for Systems and Robotics
Dept. of Electrical and Computer Engineering
University of Coimbra, Portugal
jpbar@deec.uc.pt

Abstract

We present a novel calibration technique for all central catadioptric cameras using images of planar grids. We adopted the well-known sphere camera model to describe the catadioptric projection. We show that, using the so-called lifted coordinates, a linear relation mapping the grid points to the corresponding points on the image plane can be written as a 6×6 matrix H_{cata}, which acts like the classical 3×3 homography for perspective cameras. We show how to compute the image of the absolute conic (IAC) from at least 3 homographies and how to recover from it the intrinsic parameters of the catadioptric camera. In the case of paracatadioptric cameras one such homography is enough to estimate the IAC, thus allowing the calibration from a single image.

1. Introduction

We present a novel, general, homography-based calibration algorithm for central catadioptric cameras that resembles the traditional calibration method adopted for perspective cameras [18, 23]. Catadioptric cameras consist of cameras placed in front of a curved mirror that allow to obtain a panoramic image of the surrounding environment. Since the projection rays are reflected by the mirror, these devices cannot, in general, be described by the classical central projection model, where all the projection rays are constrained to meet at a single point, the camera viewpoint. The projection rays are usually skew and they form a locus of viewpoints that can be modeled using *caustics* [19]. However, Baker and Nayar [2] derived a complete class of central catadioptric cameras: the single viewpoint constraint is preserved if the camera viewpoint is placed in one of the foci of a quadric of revolution mirror. The most useful ones are the *paracatadioptric* and the *hyper-catadioptric* models, employing a paraboloidal/hyperboloidal shape mirror coupled with an orthographic/perspective camera. Later, Geyer and Daniilidis [8] proposed a unified sphere model for describing all central catadioptric cameras: they showed that the catadioptric projection can be described by a two steps mapping, first through a unit sphere and then through a perspective camera.

Just like the traditional perspective camera, calibration of catadioptric cameras is a fundamental task. Various techniques for calibrating central cameras have been suggested; an early work by Geyer and Daniilidis [9] aimed at calibrating paracatadioptric cameras from images of lines. Barreto and Araujo extended this procedure to general central catadioptric systems [4] while Ying and Hu [20] used geometric invariants provided by lines and spheres to calibrate central catadioptric cameras. However, the calibration based on line images is usually difficult to use in practice because it requires the fitting of a conic starting from a small arc, which makes it quite inaccurate and unreliable. In general, if many lines are involved, it is difficult to solve the 2D-3D correspondence because not all the conics are images of lines. However, Barreto and Araujo determined some sufficient properties that a conic curve must satisfy to correspond to a paracatadioptric line image [3].

Some attempts to calibrate catadioptric cameras using a planar grid as in the standard perspective case [18, 23] have been proposed. Scaramuzza *et al.* [16] assumed that the image projection function can be described by a Taylor series expansion whose coefficients are estimated by solving a two-step linear least-squares minimization problem. Mei *et al.* [13] developed a calibration algorithm based on the sphere camera model adding non-linearity such as lens distortion. As input provided by the user, they used planar grids, the mirror border and the image of a non-radial line that are used to initialize the main parameters of the camera. Then the whole model is estimated through a global minimization. Recently, Zhang *et al.* [22] proposed an homography based method for calibrating a paracatadioptric camera whose orthographic camera is supposed to be calibrated a priori. They derived a homography-like relationship between the image plane and the planar grid that encodes the extrinsic parameters and the mirror parameters. Estimating the homography through 2D-2D correspondences between image points and points on a grid allows to recover all the parameters in a DLT-like procedure [1].

Recently Sturm and Barreto [17] showed that the sphere camera model can be expressed through a linear relationship, valid for any central catadioptric system. Resembling the classical pinhole projection expression, they used the so-called *lifted coordinates* to derive a generic projection matrix P_{cata}, a 6×10 matrix that maps a 3D point to the plane im-

age. Bastanlar *et al.* [6] then showed how to compute P*cata* from 3D-2D correspondences using a straightforward DLT-like approach. Then, by decomposing the estimated matrix, intrinsic and extrinsic parameters can be estimated. Such estimates can be used as initial values in an optimization step based on minimizing the reprojection error.

Our work is based on the work of Sturm and Barreto and is aimed at developing a plane-based calibration algorithm that is analogous to Zhang's [23] and Sturm *et al.*'s [18] classical approach for pinhole cameras. We show that the points on a plane are mapped into image points through a 6×6 matrix H*cata* that acts in a similar manner to the 3×3 homography matrix for classical perspective cameras. We show how to compute H*cata* from at least 12 2D-2D correspondences using a DLT approach. As it has been proved in [4, 20, 21], the image of the absolute conic depends only on the intrinsic parameters of the camera in the catadioptric system (*i.e.* it is independent of the mirror): we show that three catadioptric homographies are enough to estimate it. Once the intrinsics are estimated, all the other parameters can be derived by decomposing H*cata*. Other non-linearities, *e.g.* lens distortion, can be taken into account in a final optimization step that minimizes the reprojection error. Finally, we treat the case of paracatadioptric cameras: we show that H*cata* is rank deficient because of the degenerate configuration of the camera viewpoint which lies on the unit sphere. We prove that the left null space of H*cata* encodes all the intrinsic parameters of the camera and this allows to calibrate the catadioptric camera from a single image of a planar grid.

The paper is organized as follows. In §2 we recall some preliminary notions that will be used in §3 to derive the catadioptric homography matrix. In §4 we derive a general calibration procedure that can be applied to any central catadioptric camera, while in §5 we show that in the case of paracatadioptric cameras one homography is enough to fully calibrate the camera. §6 presents some experimental results that validate our approach while §7 concludes the paper.

2. Preliminary Notions

In this paper we represent matrices in uppercase typewriter font (M) and vectors by bold symbols (**Q**); equality of matrices or vectors up to a scale factor is expressed by $\sim$ while $[\mathbf{a}]_\times$ denotes the skew-symmetric matrix associated with the cross product.

The derivation of the catadioptric homography requires the use of lifted coordinates. The Veronese map $V_{n,d}$ of degree d maps points of $\mathcal{P}^n$ into points of an m dimensional projective space $\mathcal{P}_m$, with $m = \binom{n+d}{d} - 1$.

Consider the second order Veronese map $V_{2,2}$, that embeds the projective plane into the 5D projective space, by lifting the coordinates of point $\mathbf{q}$ to

$$\widehat{\mathbf{q}} = \left[q_1^2,\ q_1q_2,\ q_2^2,\ q_1q_3,\ q_2q_3,\ q_3^2\right]^\mathsf{T}. \qquad (1)$$

Vector $\widehat{\mathbf{q}}$ and matrix $\mathbf{qq}^\mathsf{T}$ are composed by the same ele-

ments. The former can be derived from the latter through a suitable re-arrangement of parameters. Define $\mathbf{v}(\mathtt{U})$ as the vector obtained by stacking the columns of a generic matrix U [12]. For the case of $\mathbf{qq}^\mathsf{T}$, $\mathbf{v}(\mathbf{qq}^\mathsf{T})$ has several repeated elements because of matrix symmetry. By left multiplication with a suitable permutation matrix S that adds the repeated elements, it follows that

$$\widehat{\mathbf{q}} = \mathtt{D}^{-1} \underbrace{\begin{bmatrix} 1 & 0 & 0 & 0 & 0 & 0 & 0 & 0 & 0 \\ 0 & 1 & 0 & 1 & 0 & 0 & 0 & 0 & 0 \\ 0 & 0 & 0 & 0 & 1 & 0 & 0 & 0 & 0 \\ 0 & 0 & 1 & 0 & 0 & 0 & 1 & 0 & 0 \\ 0 & 0 & 0 & 0 & 0 & 1 & 0 & 1 & 0 \\ 0 & 0 & 0 & 0 & 0 & 0 & 0 & 0 & 1 \end{bmatrix}}_{\mathtt{S}} \mathbf{v}(\mathbf{qq}^\mathsf{T}),$$

with D a diagonal matrix, $D_{ii} = \sum_{j=1}^9 S_{ij}$. If U is symmetric, then it is uniquely represented by $\mathbf{v}_{sym}(\mathtt{U})$, the row-wise vectorization of its lower left triangular part:

$$\mathbf{v}_{sym}(\mathtt{U}) = \mathtt{D}^{-1}\mathtt{S}\mathbf{v}(\mathtt{U}) = \left[U_{11},\ U_{21},\ U_{22},\ U_{31},\ \dots,\ U_{nn}\right]^\mathsf{T}.$$

In the particular case of U being symmetric and defined by two points **q** and **r**, *i.e.* $\mathtt{U} = \mathbf{qr}^\mathsf{T} + \mathbf{rq}^\mathsf{T}$, we will assume that

$$\mathbf{v}_{sym}(\mathbf{q}, \mathbf{r}) = \mathbf{v}_{sym}(\mathbf{qr}^\mathsf{T} + \mathbf{rq}^\mathsf{T}).$$

Let us now discuss the lifting of linear transformations. Consider A such that $\mathbf{r} = \mathtt{A}\mathbf{q}$. The relation $\mathbf{rr}^\mathsf{T} = \mathtt{A}(\mathbf{qq}^\mathsf{T})\mathtt{A}^\mathsf{T}$ can be written as a vector mapping

$$\mathbf{v}(\mathbf{rr}^\mathsf{T}) = (\mathtt{A} \otimes \mathtt{A})\mathbf{v}(\mathbf{qq}^\mathsf{T}),$$

with $\otimes$ denoting the Kronecker product [12]. Using the symmetric vectorization, we have $\widehat{\mathbf{q}} = \mathbf{v}_{sym}(\mathbf{qq}^\mathsf{T})$ and $\widehat{\mathbf{r}} = \mathbf{v}_{sym}(\mathbf{rr}^\mathsf{T})$, thus:

$$\widehat{\mathbf{r}} = \underbrace{\mathtt{D}^{-1}\mathtt{S}(\mathtt{A} \otimes \mathtt{A})\mathtt{S}^\mathsf{T}}_{\widehat{\mathtt{A}}}\ \widehat{\mathbf{q}}.$$

We have just derived the expression for lifting linear transformations. A has a lifted counterpart $\widehat{\mathtt{A}}$ such that $\mathbf{r} = \mathtt{A}\mathbf{q}$ iff $\widehat{\mathbf{r}} = \widehat{\mathtt{A}}\widehat{\mathbf{q}}$. For the case of a second order Veronese map, the lifting of a 2D projective transformation A is $\widehat{\mathtt{A}}$ of size 6×6. This lifting generalizes to any projective transformation, independently of the dimensions of its original and target spaces, *i.e.* it is also applicable to rectangular matrices.

In this paper we use the following liftings: 3-vectors **q** to 6-vectors $\widehat{\mathbf{q}}$, 4-vectors **Q** to 10-vectors $\widehat{\mathbf{Q}}$, 3×3 matrices K to 6×6 ones $\widehat{\mathtt{K}}$, and 3×4 matrices T to 6×10 ones $\widehat{\mathtt{T}}$.

2.1. Calibration of perspective cameras

We briefly recall the main concepts behind the homography-based calibration algorithm for standard perspective cameras as described in [10, 18, 23]. The algorithm exploits the fact that the image of the absolute conic ω (IAC) depends only on the intrinsic parameters of the camera encoded in the perspective calibration matrix K, and, in particular, it can be proven that $\omega \sim \mathtt{K}^{-\mathsf{T}}\mathtt{K}^{-1}$. Given at least three

squares not lying on parallel planes, the relevant homographies can be estimated. We recall that the 2D plane-to-image homography for perspective cameras is

$$\mathtt{H}_{3\times 3} \sim \mathtt{K} \begin{bmatrix} \mathbf{R}_1 & \mathbf{R}_2 & \mathbf{t} \end{bmatrix}, \qquad (2)$$

where $\mathbf{R}_i$ is the i-th column of the rotation matrix $\mathtt{R}$ and $\mathbf{t}$ the translation vector of the pose matrix. For each estimated homography, the images of the circular points of the respective plane can be computed and used to fit the conic ω. Finally the calibration matrix $\mathtt{K}$ and its intrinsic parameters can be computed from ω using, *e.g.*, the Cholesky factorization. The pose matrices can be recovered by decomposing the homographies according to (2). In the following two sections an analogous procedure will be proposed for central catadioptric cameras.

3. Catadioptric Homography

In this section we use and extend material proposed by [17]. According to the sphere based model [8], all central catadioptric cameras can be modeled by a unit sphere and a perspective camera, such that the projection of a 3D point can be performed in two steps (see Figure 1). First, the point is projected onto the sphere w.r.t. its center to two antipodal points, $\mathbf{S}_+$ and $\mathbf{S}_-$. Then, those points are projected through the perspective camera into two image points $\mathbf{q}_+$ and $\mathbf{q}_-$. The distance ξ between the perspective camera and the center of the sphere determines the type of catadioptric camera, *e.g.* $\xi = 0$ for perspective, $\xi = 1$ for paracatadioptric, $0 < \xi < 1$ for hypercatadioptric. Note that even for the paracatadioptric case, where the true camera is an affine one, the camera in the sphere based model is still perspective.

Let us now consider 3D points lying on a single plane (the calibration grid). Without loss of generality, let the unit sphere be located at the origin and the optical center of the perspective camera, at the point $\mathbf{C}_p = \begin{bmatrix} 0, 0, \xi \end{bmatrix}^{\mathsf{T}}$. The perspective camera is modeled by the projection matrix $\mathtt{P} \sim \mathtt{A}_p \mathtt{R}_p \begin{bmatrix} \mathtt{I} & -\mathbf{C}_p \end{bmatrix}$. For full generality, we include a rotation $\mathtt{R}_p$; this may encode an actual rotation of the true camera looking at the mirror, but may also simply be a projective change of coordinates in the image plane, like for paracatadioptric cameras, where the true camera's rotation is fixed, modulo rotation about the mirror axis. Note that all parameters of the perspective camera, *i.e.* both its intrinsic and extrinsic parameter sets, are intrinsic parameters for the catadioptric camera. Hence, we replace $\mathtt{A}_p \mathtt{R}_p$ by a generic projective transformation $\mathtt{K}$ from now on. The intrinsic parameters of the catadioptric camera are thus ξ and $\mathtt{K}$. The projection of a 3D point $\mathbf{Q}$ goes as follows. The two intersection points of the sphere and the line joining its center and $\mathbf{Q}$, are $\mathbf{S}_\pm \sim \begin{bmatrix} Q_1, Q_2, Q_3, \pm\sqrt{Q_1^2 + Q_2^2 + Q_3^2} \end{bmatrix}^{\mathsf{T}}$. Their images in the perspective camera are

$$\mathbf{q}_\pm \sim \mathtt{P}\mathbf{S}_\pm \sim \mathtt{K} \begin{bmatrix} Q_1 \\ Q_2 \\ Q_3 \pm \xi\sqrt{Q_1^2 + Q_2^2 + Q_3^2} \end{bmatrix}.$$
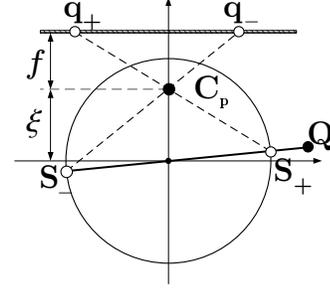

Figure 1. The sphere based model for catadioptric projection [8]. The black dot is the optical center of the perspective camera and the plane on the top its image plane.

We can represent the 2D points $\mathbf{q}_\pm$ via a single geometric entity by computing the degenerate dual conic generated by them, *i.e.* the dual conic containing exactly the lines going through at least one of the two points. The dual conic is given by $\Omega \sim \mathbf{q}_+\mathbf{q}_-^{\mathsf{T}} + \mathbf{q}_-\mathbf{q}_+^{\mathsf{T}}$, *i.e.*

$$\Omega \sim \mathtt{K} \begin{bmatrix} Q_1^2 & Q_1 Q_2 & Q_1 Q_3 \\ Q_1 Q_2 & Q_2^2 & Q_2 Q_3 \\ Q_1 Q_3 & Q_2 Q_3 & Q_3^2 - \xi^2(Q_1^2 + Q_2^2 + Q_3^2) \end{bmatrix} \mathtt{K}^{\mathsf{T}}.$$

This can be written as a linear mapping of the 3D point's lifted coordinates, onto the vectorized matrix of the conic:

$$\mathbf{v}_{sym}(\Omega) \sim \widehat{\mathtt{K}}_{6\times 6} \underbrace{\begin{bmatrix} 1 & 0 & 0 & 0 & 0 & 0 \\ 0 & 1 & 0 & 0 & 0 & 0 \\ 0 & 0 & 1 & 0 & 0 & 0 \\ 0 & 0 & 0 & 1 & 0 & 0 \\ 0 & 0 & 0 & 0 & 1 & 0 \\ -\xi^2 & 0 & -\xi^2 & 0 & 0 & 1-\xi^2 \end{bmatrix}}_{\mathtt{X}_\xi} \begin{bmatrix} \mathtt{I}_6 & \mathbf{0}_{6\times 4} \end{bmatrix} \widehat{\mathbf{Q}}_{10}.$$

$$(3)$$

Without loss of generality, we can choose a suitable world reference frame so that, *e.g.*, the points lie on the plane $z = 0$; then extrinsic parameters of the camera can be introduced, *i.e.* a pose matrix $\mathtt{T} = \mathtt{R} \begin{bmatrix} \mathtt{I}_3 & -\mathbf{t} \end{bmatrix}$ and the projection becomes

$$\mathbf{v}_{sym}(\Omega) \sim \widehat{\mathtt{K}}_{6\times 6} \, \mathtt{X}_{\xi 6\times 6} \, \widehat{\mathtt{R}}_{6\times 6} \begin{bmatrix} \mathtt{I}_6 & \mathtt{T}'_{4\times 6} \end{bmatrix} \widehat{\mathbf{Q}}_{10}, \qquad (4)$$

where $\mathtt{T}'$ depends only on $\mathbf{t}$. Since the third coordinate of each point $\mathbf{Q}$ is 0, its lifted representation $\widehat{\mathbf{Q}}$ has always 4 zero components, *i.e.* the 4th, 5th, 6th and 9th components respectively. Therefore the corresponding columns of the 6×10 matrix $\begin{bmatrix} \mathtt{I}_6 & \mathtt{T}'_{4\times 6} \end{bmatrix}$ can be dropped and each point on the plane is mapped on the image plane through the following matrix

$$\mathtt{H}_{cata} \sim \widehat{\mathtt{K}} \, \mathtt{X}_\xi \, \widehat{\mathtt{R}} \begin{bmatrix} \mathtt{I}_{6\times 3} & \begin{bmatrix} \mathbf{t}'_1 & \mathbf{t}'_2 & \mathbf{t}'_4 \end{bmatrix} \end{bmatrix}, \qquad (5)$$

where $\mathbf{t}'_i$ is the i-th column of the matrix $\mathtt{T}'$ and $\mathtt{H}_{cata}$ is the 6×6 homography matrix relating the lifting of the 2D coordinates of the points on the plane to their dual conic representation on the image plane. Comparing $\mathtt{H}_{cata}$ with $\mathtt{H}$ in (2), we can note a similar structure for the two matrices. We also remind that, in order to estimate $\mathtt{H}$, at least 4 2D-2D point correspondences allow to set up linear equations on $\mathtt{H}$ by imposing $[\mathbf{q}]_\times \mathtt{H}\mathbf{Q} = \mathbf{0}$ [10]. In the catadioptric case, the homography

H$_{cata}$ cannot be estimated directly by comparing a space point $\mathbf{Q}$ with its image point $\mathbf{q}$, since H maps $\mathbf{Q}$ into a degenerate dual conic Ω "containing" $\mathbf{q}$. On the other hand, $\mathbf{q}$ must be one of the generators of Ω, so that any line through $\mathbf{q}$ must lie on Ω. Hence $\forall \mathbf{p} : \mathbf{p} \times \mathbf{q} \in \Omega$, *i.e.* $\mathbf{p}^{\mathsf{T}} [\mathbf{q}]_{\times} \Omega [\mathbf{q}]_{\times} \mathbf{p} = 0$, which gives $[\mathbf{q}]_{\times} \Omega [\mathbf{q}]_{\times} = 0_{3\times3}$. Expressing the constraint with the lifted coordinates it yields to

$$\left(\widehat{[\mathbf{q}]_{\times}}\right)_{6\times6} \mathbf{v}_{sym}(\Omega) = \widehat{[\mathbf{q}]_{\times}} \, \mathtt{H}_{cata} \, \widehat{\mathbf{Q}}_6 = \mathbf{0}_6.$$

This is a linear expression that allows to estimate H$_{cata}$ from point correspondences using, *e.g.*, a standard DLT-like approach. While a 3×3 skew symmetric matrix has rank 2, its lifted version has rank 3; therefore each correspondence can provide 3 linear constraints on the 35 parameters of H$_{cata}$. Hence the catadioptric homography can be estimated with a minimum of 12 matches.

3.1. Image-to-Plane Homography

The homography H$_{cata}$ maps a point on the grid to the dual degenerate conic coding the two projected image points. The reciprocal mapping between image points and points on the plane is not the inverse of H$_{cata}$. In the following we derive an expression for the image-to-plane homography. This is for completeness; it is not used in our calibration algorithm.

Consider an image point $\mathbf{q}$ and its backprojection. First $\mathbf{q}$ is backprojected w.r.t. the perspective camera, giving a 3D line that intersects the sphere in two points. The two backprojection rays are the two lines spanned by the origin and the intersection points, *i.e.* the lines $\mathbf{L}_{\pm}$ going through the center of the sphere and the points $\mathbf{S}_{\pm} = \left[\mathbf{b}_{\pm}^{\mathsf{T}}, \, 1\right]^{\mathsf{T}}$, where

$$\mathbf{b}_{\pm}^{\mathsf{T}} = \left(\mathbf{r}^{\mathsf{T}}\mathbf{r}\right) \mathbf{C}_p + \left(\xi r_3 \pm \sqrt{\xi^2 r_3^2 - \left(\mathbf{r}^{\mathsf{T}}\mathbf{r}\right)\left(\xi^2 - 1\right)}\right) \mathbf{r},$$

with $\mathbf{r} \sim \mathtt{K}^{-1}\mathbf{q}$. Without loss of generality we can assume the world reference frame set so that the grid lies on the plane $z = 0$. Then the two backprojection lines $\mathbf{L}_{\pm}$ can be expressed w.r.t. the world reference system as $\mathbf{L}_{\pm}^w = \mathbf{t} + \lambda \mathtt{R}\mathbf{b}_{\pm}$, where $\mathbf{t}$ and $\mathtt{R}$ are the components of the pose matrix. The backprojection lines intersect the grid in two points: the 3rd coordinate of such points is always 0, therefore we can derive the value of λ by imposing that the 3rd coordinate of $\mathbf{L}_{\pm}^w$ is zero, thus obtaining $\lambda_{\pm} = -\frac{t_3}{\mathtt{R}_3 \mathbf{b}_{\pm}}$. Substituting $\lambda_{\pm}$ in $\mathbf{L}_{\pm}^w$, we obtain the two 2D points on the grid

$$\mathbf{Q}_{\pm} = \begin{bmatrix} t_1\mathbf{R}_3 - t_3\mathbf{R}_1 \\ t_2\mathbf{R}_3 - t_3\mathbf{R}_2 \\ \mathbf{R}_3 \end{bmatrix} \mathbf{b}_{\pm} = \mathtt{A}_{3\times3}\mathbf{b}_{\pm},$$

where $\mathbf{R}_i$ is the i-th row of R. We can represent the two points through the associated degenerate dual conic

$$\Omega \sim \mathbf{Q}_+\mathbf{Q}_-^{\mathsf{T}} + \mathbf{Q}_-\mathbf{Q}_+^{\mathsf{T}} \sim \mathtt{A}\mathbf{b}_+\left(\mathtt{A}\mathbf{b}_-\right)^{\mathsf{T}} + \mathtt{A}\mathbf{b}_-\left(\mathtt{A}\mathbf{b}_+\right)^{\mathsf{T}}$$
$$\sim \mathtt{A}\left(\mathbf{b}_+\mathbf{b}_-^{\mathsf{T}} + \mathbf{b}_-\mathbf{b}_+^{\mathsf{T}}\right)\mathtt{A}^{\mathsf{T}},$$

that can be written as a linear mapping of the 2D point's lifted coordinates

$$v_{sym}(\Omega) \sim \widehat{\mathtt{A}}\mathtt{B}_\xi\widehat{\mathbf{r}} \sim \underbrace{\widehat{\mathtt{A}}\mathtt{B}_\xi\widehat{\mathtt{K}}^{-1}}_{\mathtt{H}_{i2p}}\widehat{\mathbf{q}} \sim \mathtt{H}_{i2p}\widehat{\mathbf{q}}, \qquad (6)$$

where

$$\mathtt{B}_\xi = \begin{bmatrix} \xi^2 - 1 & 0 & 0 & 0 & 0 & 0 \\ 0 & \xi^2 - 1 & 0 & 0 & 0 & 0 \\ 0 & 0 & \xi^2 - 1 & 0 & 0 & 0 \\ 0 & 0 & 0 & -1 & 0 & 0 \\ 0 & 0 & 0 & 0 & -1 & 0 \\ \xi^2 & 0 & \xi^2 & 0 & 0 & -1 \end{bmatrix}.$$

The 6×6 matrix H$_{i2p}$ is the homography mapping the image points into a degenerate dual conic generated by the two world points $\mathbf{Q}_{\pm}$ on the plane. The matrix H$_{i2p}$ can be estimated from 12 points with a DLT approach just like H$_{cata}$.

4. Homography-Based Catadioptric Calibration

In this section we derive a homography-based calibration algorithm for catadioptric cameras that is similar in spirit to the one for perspective cameras (see §2.1). To this end and for the sake of completeness, we briefly recall the catadioptric projection of the circular points and of the absolute conic [4, 20, 21].

Circular point projection. What is the image of the scene plane's circular points under the general projection model (4)? The circular points $\mathbf{J}_{\pm} = \begin{bmatrix} 1 & \pm i & 0 \end{bmatrix}^{\mathsf{T}}$ project on the unitary sphere into themselves. Indeed, any sphere intersects the plane at infinity at the absolute conic; since the circular points belong to the absolute conic, they also belong to the sphere. Each circular point is projected through the perspective projection of the sphere model in a single point on the image plane

$$\mathbf{q}_{\pm} \sim \mathtt{K} \begin{bmatrix} \mathtt{I}_3 & -\mathbf{C}_p \end{bmatrix} \begin{bmatrix} \mathtt{R}\,\mathbf{J}_{\pm} \\ 0 \end{bmatrix} \sim \mathtt{K}\mathtt{R}\,\mathbf{J}_{\pm},$$

from which we can remark that the projection of the circular points is independent of ξ. If we project a circular point with H$_{cata}$ we obtain the lifted representation of a dual degenerate conic of rank 1, *i.e.* a dual conic containing all the lines passing through a given point, the image of the circular point.

Absolute conic projection. Straightforwardly, any point of the absolute conic projects on the sphere into itself and in a (repeated) point on the image plane. Similarly to circular points it can be easily proven that the projection of the absolute conic is also independent of ξ. The absolute conic is then projected as in the standard perspective case and the relationship $\omega \sim \mathtt{K}^{-\mathsf{T}}\mathtt{K}^{-1}$ still holds. Moreover, since we assumed $\mathtt{K} = \mathtt{A}_p\mathtt{R}_p$, it yields

$$\omega \sim \mathtt{K}^{-\mathsf{T}}\mathtt{K}^{-1} \sim \mathtt{A}_p^{-\mathsf{T}}\mathtt{R}_p^{-\mathsf{T}}\mathtt{R}_p^{-1}\mathtt{A}_p^{-1} \sim \mathtt{A}_p^{-\mathsf{T}}\mathtt{A}_p^{-1},$$

$$M \sim X_\xi \widehat{R} I_{6\times3} \sim \begin{bmatrix} \widehat{R}_{11} & \widehat{R}_{12} & \widehat{R}_{13} \\ \widehat{R}_{21} & \widehat{R}_{22} & \widehat{R}_{23} \\ \widehat{R}_{31} & \widehat{R}_{32} & \widehat{R}_{33} \\ \widehat{R}_{41} & \widehat{R}_{42} & \widehat{R}_{43} \\ \widehat{R}_{51} & \widehat{R}_{52} & \widehat{R}_{53} \\ \widehat{R}_{61} - \left(\widehat{R}_{11} + \widehat{R}_{31} + \widehat{R}_{61}\right)\xi^2 & \widehat{R}_{62} - \left(\widehat{R}_{12} + \widehat{R}_{32} + \widehat{R}_{62}\right)\xi^2 & \widehat{R}_{63} - \left(\widehat{R}_{11} + \widehat{R}_{33} + \widehat{R}_{63}\right)\xi^2 \end{bmatrix}$$

Figure 2. The matrix M.

i.e. the IAC only depends on the intrinsic parameters of the perspective camera in the sphere model. Hence the calibration algorithm for central catadioptric cameras can be inspired by the one for the perspective case. The projections of the circular points from at least 3 images can be used to fit a conic (the IAC) and then to perform the Cholesky factorization to retrieve A_p. The catadioptric parameter ξ and the pose matrices can be derived by decomposing the homography matrices according to (5). For a first rough estimate of the parameters, we can neglect the camera rotation matrix and then assume $R_p = I$, so that $K = A_p$. Then we observe that we can eliminate the calibration matrix from the homography by multiplying the matrix H_{cata} by the inverse of K:

$$\widehat{K}^{-1} H_{cata} \sim X_\xi \widehat{R} \left[I_{6\times3} \; \left[\mathbf{t}'_1 \; \mathbf{t}'_2 \; \mathbf{t}'_4 \right] \right].$$

Consider now the leftmost 6×3 submatrix $M \sim X_\xi \widehat{R} I_{6\times3}$ (see Figure 2) and let N be the corresponding leftmost 6×3 submatrix of $\widehat{K}^{-1} H_{cata}$: since the catadioptric parameter ξ appears only in the last row of X_ξ, only the elements of the last row of M contain ξ. We can exploit this to extract the value of ξ. Since M is equal to N up to a scalar factor, we can set up the following equations

$$N_{61} = \lambda M_{61} = \lambda \left(\widehat{R}_{61} - \left(\widehat{R}_{11} + \widehat{R}_{31} + \widehat{R}_{61} \right) \xi^2 \right)$$
$$N_{62} = \lambda M_{62} = \lambda \left(\widehat{R}_{62} - \left(\widehat{R}_{12} + \widehat{R}_{32} + \widehat{R}_{62} \right) \xi^2 \right)$$
$$N_{63} = \lambda M_{63} = \lambda \left(\widehat{R}_{63} - \left(\widehat{R}_{11} + \widehat{R}_{33} + \widehat{R}_{63} \right) \xi^2 \right)$$

All the elements of $\widehat{R}_{ij}$ in these equations can be inferred from M but the $\widehat{R}_{6j}$, for which it can be proven that the following relationships hold:

$$\widehat{R}_{61} = \frac{\widehat{R}_{41}\widehat{R}_{51}}{\widehat{R}_{21}}, \; \widehat{R}_{62} = \frac{2\widehat{R}_{41}\widehat{R}_{42} - \widehat{R}_{61}\widehat{R}_{12}}{\widehat{R}_{11}}, \; \widehat{R}_{63} = \frac{\widehat{R}_{43}\widehat{R}_{53}}{\widehat{R}_{23}}.$$

Then, in order to eliminate the scalar factor, we can consider, *e.g.*, $\frac{N_{61}}{N_{62}} = \frac{M_{61}}{M_{62}}$ and then solve the straightforward 2nd degree equation on ξ.

This procedure allows to estimate also the rotation matrix R. Once R is known, following a similar procedure it is possible to estimate the translation vector $\mathbf{t}$.

4.1. Other Parameters

In order to fully describe a real camera, other parameters must be taken into account. As mentioned before, K contains both the camera intrinsic parameters encoded in A_p and the rotation R_p. As for the latter, we only consider rotations about the x-axis and the y-axis, since rotation about the optical axis is merged with the rotation of the entire catadioptric system about the z-axis.

We also consider distortions introduced by the camera lens. We adopt a classical distortion model introduced by [7] which is part of many calibration algorithms [11]. The radial and tangential distortion introduced by the lens shape can be approximated by the following expression

$$\mathbf{x}_d = \left(1 + k_1 r^2 + k_2 r^4 + k_3 r^6 + \ldots \right) \mathbf{x}_n + \mathbf{dx},$$

where $\mathbf{x}_n(u, v)$ are the coordinates of the normalized projected point $(f = 1)$, $r = \sqrt{u^2 + v^2}$, $\mathbf{x}_d$ are the coordinates of the distorted point, and $\mathbf{dx}$ is the tangential distortion vector

$$\mathbf{dx} = \left[2l_1 uv + l_2(r^2 + 2u^2), \; l_1(r^2 + 2v^2) + 2l_2 uv \right]^\mathsf{T}.$$

We use 3 coefficients to describe the radial distortion and 2 for the tangential component, so that the lens distortion is described by the 5 parameters $[k_1, k_1, k_3, l_1, l_2]$. All these additional parameters are initialized as zero.

4.2. Non-Linear Optimization

The whole model is fully described by $11 + 6n$ parameters where $n \geq 3$ is the number of images. The camera is described by the focal length f, the principal point c_x and c_y, the rotation parameters θ_x and θ_y, the distortion parameters $[k_1, k_1, k_3, l_1, l_2]$, and the catadioptric parameter ξ. Then for each image the 6 parameters of the pose matrix have to be estimated.

Once the initial values of the parameters have been estimated from the homographies, a non-linear optimization can be run in order to refine their estimation and to estimate all the remaining parameters. However, due to the large number of variables involved and the possibly poor estimation of the initial values, we have experienced that the non-linear optimization step does not converge to the optimal solution but gets often stuck in local minima. In order to improve the optimization step we split it into three parts that work in cascades.

The first step aims at improving and refining the initial A_p values: we have experienced that the calibration matrix is usually well estimated while ξ and the pose matrices are not. Therefore, for each image, we run a brief optimization step to refine the values of the pose matrix according to the esti-

mated ξ and K. For each image point the backprojection rays are computed and the optimal extrinsic parameters that allow to align the points on the plane with the associated backprojection rays are estimated. As minimization criterion we use the norm cross product between the direction of the ray and the direction of the 3D point on the plane.

The second step is similar to the previous one but relaxes the constraint on ξ being fixed. We consider all the images together and we try to find the optimal values of ξ and of the extrinsics that best fit the hypothesis on K, supposed to be fixed. For all the images the optimization step minimizes the cross product between the direction of the 3D points and the direction of the associated backprojection rays. At the end of this step we thus obtain the optimal values of the parameters according to the estimated K.

Finally, in the third step a final non-linear optimization step minimizes the reprojection error taking into account all the other parameters that have been neglected before. The initial values for these parameters are usually set by default as 0. We use the Levenberg-Marquardt method assuming as minimization criterion the root mean square (RMSe) of distance error between the image points and their projected counterparts[1]. Derivatives of the cost function are computed numerically.

5. Paracatadioptric Homography

In the paracatadioptric case we have $\xi = 1$ and the camera viewpoint lies on the sphere itself. This introduces some degeneracies in the projection equation, *e.g.* the matrix X_ξ (3) becomes rank deficient and H_{cata} has rank 5. Moreover, consider a point $\mathbf{Q}$ and its two associated projection rays $\mathbf{s}_+$ and $\mathbf{s}_-$ in the perspective camera in the sphere model, *i.e.* the projection rays associated to the points $\mathbf{S}_\pm$ w.r.t. the center of projection $\mathbf{C}_p$ in Figure 1. These two rays are always perpendicular due to the basic properties of the sphere. We can express this relationship as $\mathbf{s}_+^\mathsf{T} I_3 \mathbf{s}_- = 0$, which can be written using the lifted representation as

$$\mathbf{v}_{sym}(I_3)^\mathsf{T} D_6 \mathbf{v}_{sym}(\mathbf{s}_+, \mathbf{s}_-) = 0.$$

Since $\mathbf{s}_+$ and $\mathbf{s}_-$ are perpendicular, their two corresponding image points $\mathbf{q}_+$ and $\mathbf{q}_-$ must be harmonic w.r.t. the IAC. Let us denote $\widehat{\omega}$ its lifted representation, it follows that

$$\widehat{\omega}^\mathsf{T} D_6 \mathbf{v}_{sym}(\mathbf{q}_+, \mathbf{q}_-) = \widehat{\omega}^\mathsf{T} D_6 H_{cata} \widehat{\mathbf{Q}} = \mathbf{0} \quad \forall \mathbf{Q} \in \mathcal{P}^3.$$

Since this equation must hold for any point $\mathbf{Q}$, the IAC can be directly computed using the left null space of the homography matrix:

$$\widehat{\omega}^\mathsf{T} \sim D_6^{-1} \mathcal{N}(H_{cata}^\mathsf{T}). \tag{7}$$

This allows to calibrate a paracatadioptric camera from a single image of a plane: once the homography has been estimated, the IAC can be computed from it through (7). Then

---

[1]Since the catadioptric projection (5) always gives two points on the image plane, in order to compute the distance error we choose the projected point closer to the point measured on the image.

the same approach described before for the general case can be applied to compute the other parameters.

5.1. Image-to-Plane Paracatadioptric Homography

For the sake of completeness we briefly report how to derive the reciprocal mapping for paracatadioptric cameras between image points and points on the plane as it has been shown in [5]. Considering the backprojection of an image point in the case of a paracatadioptric camera, one of the intersection points is always the camera center. Therefore all image points share a common backprojection ray, *i.e.* the axis going through the center of the sphere and the camera viewpoint. According to the inverse stereographic projection [14], the homogeneous coordinates of the second intersection point on the sphere are

$$\mathbf{P} \sim \begin{bmatrix} 2r_1r_3, & 2r_2r_3, & r_3^2 - r_1^2 - r_2^2, & -r_3^2 - r_1^2 - r_2^2 \end{bmatrix}^\mathsf{T},$$

with $\mathbf{r} \sim K^{-1}\mathbf{q}$. Writing the coordinates of $\mathbf{P}$ using the lifted coordinates we get

$$\mathbf{P} \sim \begin{bmatrix} 0 & 0 & 0 & 2 & 0 & 0 \\ 0 & 0 & 0 & 0 & 2 & 0 \\ -1 & 0 & -1 & 0 & 0 & 1 \\ -1 & 0 & -1 & 0 & 0 & -1 \end{bmatrix} \widehat{K}^{-1}\widehat{\mathbf{q}}.$$

Without loss of generality we can assume a suitable world reference system for the points on the plane so that they lie on the plane $z = 0$. It can be proven that the following expression holds

$$H_{i2p} \sim H_{3 \times 3}^{-1} \begin{bmatrix} 0 & 0 & 0 & 2 & 0 & 0 \\ 0 & 0 & 0 & 0 & 2 & 0 \\ -1 & 0 & -1 & 0 & 0 & 1 \end{bmatrix} \widehat{K}^{-1}, \tag{8}$$

where H is the matrix

$$H \sim \begin{bmatrix} \mathbf{R}_1 & \mathbf{R}_2 & \mathbf{t} \end{bmatrix}$$

containing the first two columns of the rotation matrix R and the translation vector $\mathbf{t}$ of the pose matrix. The matrix H_{i2p} is the 3×6 paracatadioptric homography mapping the lifted coordinates of the image point $\mathbf{q}$ to the (homogeneous) coordinates of the corresponding point on the plane.

6. Experimental Results

In this section we present some experimental results in calibrating the two most common types of catadioptric cameras. We considered two image datasets, one taken with a paracatadioptric camera and the other with a hyberboloidal-based catadioptric camera. As calibration pattern we used a classical check board from which we estimated H_{cata}. A first estimate was obtained with 12 initial points selected manually. Then the estimate can be refined with an iterative procedure employing image processing techniques (Figure 3). Such a procedure, which is very common for perspective cameras, has not been possible until now for non-conventional im-
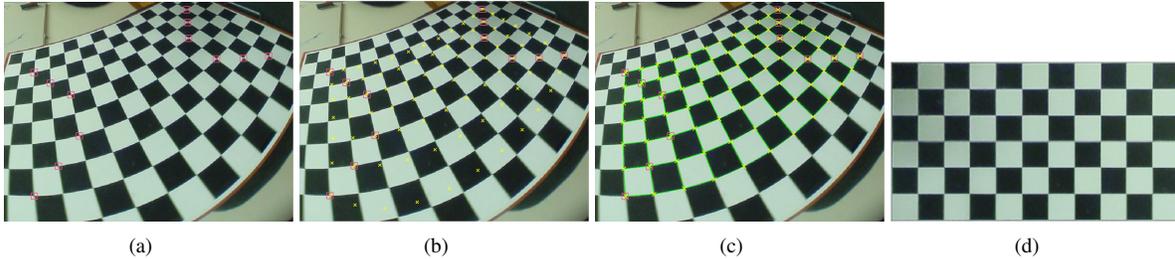
Figure 3. (a) 12 points (red markers) are manually selected and the homography estimated. (b) Using the estimated homography the grid is projected on the image (yellow crosses) to identify other points and re-estimate the homography. (c) After 5 iterations all the points are well identified and H_{cata} gives a reprojection error (RMSe) of 0.14 pixels. (d) The homography allows to unwarp the (uncalibrated) image of the grid.

agery, unless other initial information is provided by the user [13].

In order to evaluate the calibration results we compare our results with the one obtained by calibrating the same datasets with the toolbox provided by [13]. Since the projection models are slightly different, we cannot directly compare the estimated parameters, but we rather compared the results via cross-validation using the reprojection error using RMSe and standard deviation. For each dataset we proceeded as follows. We first calibrated the camera using all the available images. Then we repeated the calibration procedure over subsets of images, using the remaining ones as validation set: *e.g.* in a dataset of 10 images, we first perfomed the calibration with all the 10 images, then we used 9 images to calibrate and 1 for validation, then 8 and 2 and so on. Cross-validation was performed by estimating the pose of these validation images, and then computing reprojection errors. At each stage, we repeated the calibration 10 times over different combinations of images and then we considered the mean RMSe and the relevant standard deviation. In this way we could evaluate the reliability and the accuracy of the calibration according to the number of images used.

Paracatadioptric Camera. The paracatadioptric dataset is a publicly available set of 10 images with a resolution of 1280×1024[15]. It is worth to remark that in [13] the paracatadioptric camera is treated as a special case where ξ is known and costant. This allows to ease the calibration process and the estimation of the parameters. Our approach, instead, is more general since the user is asked to provide only the initial points of the check board for homography estimation and then all the calibration parameters are recovered without any other assumption. Figure 4.a shows the reprojection error and the its standard deviation for the images used for calibration. Figure 4.b shows the RMSe for the cross-validation images and one can notice that the error increases as less images are used in the calibration process. Our approach performed well and the accuracy is better than the one obtained with the method [13]. It is worth to note that, when compared to [13], our method has significant better reprojection errors on the cross-validation images.

Finally, Figure 4.c shows the RMSe on calibration images when calibrating the paracatadioptric camera with just a single image of the dataset: the performance varies with the image considered but, overall, the RMSe are comparable with the previous ones.

Hypercatadioptric Camera. The dataset is taken with a hypercatadioptric camera and is composed of 6 images with a resolution of 1024×768. Even in this case our method perfomed well showing an RMSe on the images used for calibration always comparable with the ones of [13] (Figure 4.d) and a slightly better RMSe on the cross-validation images (Figure 4.e). Finally, Figure 4.f shows the mean estimate for ξ: while in [13] the value of ξ varies significantly according to the number of images used, using our approach we observed a better stability; the estimated value of ξ that remains rather constant over all trials.

7. Conclusions

We presented a novel approach for calibrating any central catadioptric camera from images of planes. We have derived the formulation of a 6×6 catadioptric homography that, using the lifted coordinates, maps a point on the plane to its two theoretical images on the image plane. Similarly to the case of perspective cameras, we have shown that the image of the absolute conic contains the intrinsic parameters of the perspective camera and we have devised a procedure to extract all the other parameters by decomposing the homography. We have also shown that in the case of a paracatadioptric camera, due to the inner degeneracies of the model, the calibration can always be performed just from a single image. Experimental results show the effectiveness of our approach, even when compared with the method proposed in [13].
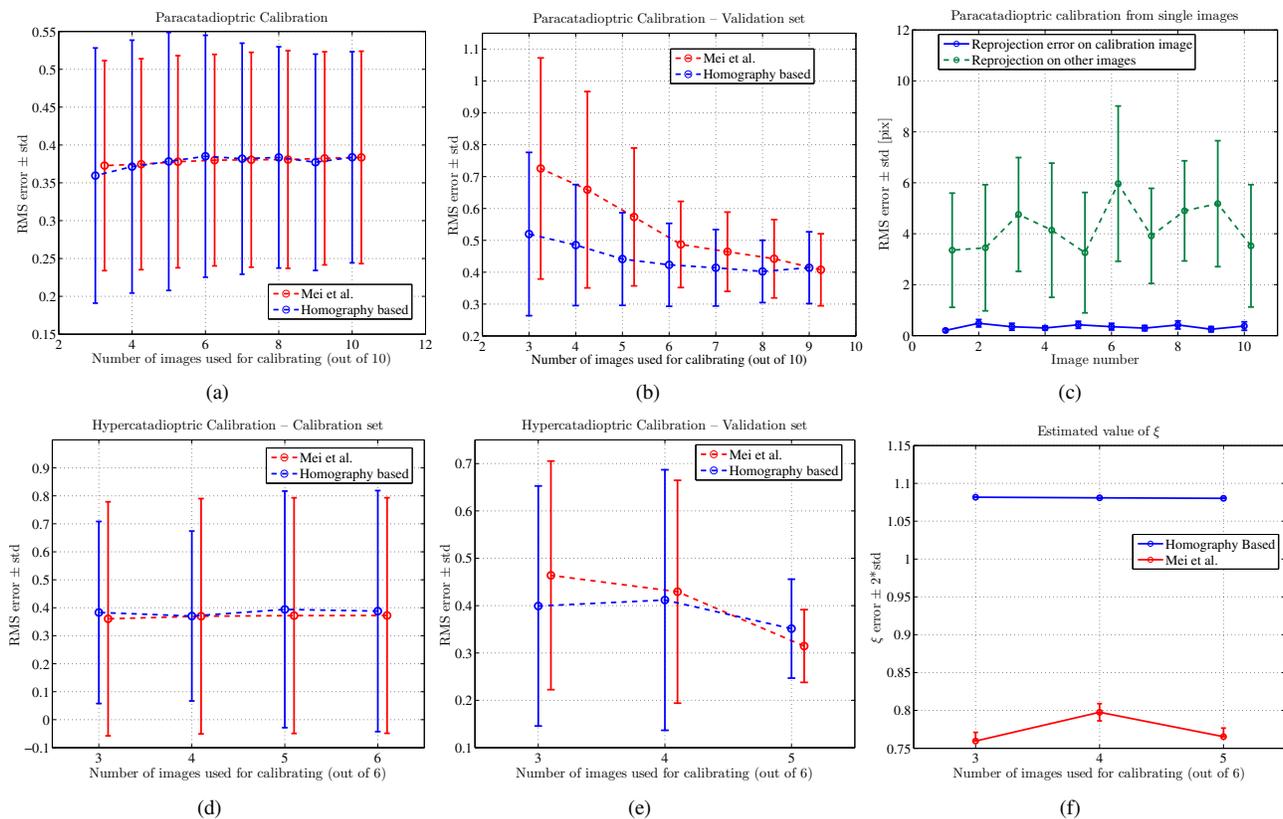
Figure 4. **Top row, paracatadioptric calibration:** reprojection error RMSe and its standard deviation of the images used for calibration (a) and for cross-validation (b). (c) Single image calibration: reprojection error RMSe and its standard deviation on calibration images (blue) and other images of the dataset (dark green). **Bottom row, hypercatadioptric calibration**: reprojection error RMSe and its standard deviation of the images used for calibration (d) and for cross-validation (e). (f) The mean estimated value of ξ over different calibration sets: the estimated value of ξ is greater than 1 because no constraints are imposed in the minimization and the value of ξ is usually coupled with the focal length f.

References

[1] Y. Abdel-Aziz and H. Karara. Direct linear transformation from comparator coordinates into object space coordinates in close-range photogrammetry. In *Proceedings of the Symposium on Close-Range Photogrammetry*, pages 1–18, 1971. 1

[2] S. Baker and S. K. Nayar. A theory of single-viewpoint catadioptric image formation. *IJCV*, 35(2):175–196, 1999. 1

[3] J. Barreto and H. Araujo. Paracatadioptric camera calibration using lines. In *ICCV '03*, volume 2, pages 1359–1365, 13-16 Oct. 2003. 1

[4] J. Barreto and H. Araujo. Geometric properties of central catadioptric line images and their application in calibration. *PAMI*, 27(8):1327–1333, 2005. 1, 2, 4

[5] J. Barreto and K. Daniilidis. Epipolar geometry of central projection systems using veronese maps. In *CVPR '06*, volume 1, pages 1258–1265, 2006. 6

[6] Y. Bastanlar, L. Puig, P. Sturm, J. Guerrero, and J. Barreto. DLT-like calibration of central catadioptric cameras. In *OMNIVIS '08*, 2008. 2

[7] D. Brown. Decentering distortion of lenses. *Photogrammetric Engineering*, 32(3):444–462, 1966. 5

[8] C. Geyer and K. Daniilidis. Catadioptric projective geometry. *IJCV*, 45(3):223–243, 2001. 1, 3

[9] C. Geyer and K. Daniilidis. Paracatadioptric camera calibration. *PAMI*, 24(5):687–695, 2002. 1

[10] R. I. Hartley and A. Zisserman. *Multiple View Geometry in Computer Vision*. Cambridge University Press, second edition, 2004. 2, 3

[11] J. Heikkila and O. Silven. A four-step camera calibration procedure with implicit image correction. In *CVPR '97*, 1997. 5

[12] R. A. Horn. *Topics in matrix analysis*. Cambridge University Press, New York, NY, USA, 1986. 2

[13] C. Mei and P. Rives. Single view point omnidirectional camera calibration from planar grids. In *ICRA*, 2007. 1, 7

[14] H. Pottmann and J. Wallner. *Computational Line Geometry*. Mathematics and Visualization. Springer-Verlag New York, Inc., Secaucus, NJ, USA, 2001. 6

[15] D. Scaramuzza. Omnidirectional camera calibration toolbox for matlab. http://asl.epfl.ch/~scaramuz/research/Davide_Scaramuzza_files/Research/OcamCalib_Tutorial.htm. 7

[16] D. Scaramuzza, A. Martinelli, and R. Siegwart. A toolbox for easily calibrating omnidirectional cameras. In *IROS*, pages 5695–5701, 2006. 1

[17] P. Sturm and J. Barreto. General imaging geometry for central catadioptric cameras. In *ECCV '08*, pages 609–622, 2008. 1, 3

[18] P. Sturm and S. Maybank. On plane-based camera calibration: A general algorithm, singularities, applications. In *CVPR '99*, volume 1, pages 1432–1437, 1999. 1, 2

[19] R. Swaminathan, M. D. Grossberg, and S. K. Nayar. Non-single viewpoint catadioptric cameras: Geometry and analysis. *IJCV*, 66(3):211–229, 2006. 1

[20] X. Ying and Z. Hu. Catadioptric camera calibration using geometric invariants. *PAMI*, 26(10):1260–1271, 2004. 1, 2, 4

[21] X. Ying and H. Zha. Identical projective geometric properties of central catadioptric line images and sphere images with applications to calibration. *IJCV*, 78(1):89–105, 2008. 2, 4

[22] B. Zhang and Y. Li. Homography-based method for calibrating an omnidirectional vision system. *J. Opt. Soc. Am. A*, 25(6):1389–1394, 2008. 1

[23] Z. Zhang. A flexible new technique for camera calibration. *PAMI*, 22:1330–1334, 2000. 1, 2